Nano Energy 84 (2021) 105921

Contents lists available at ScienceDirect

Nano Energy

journal homepage: http://www.elsevier.com/locate/nanoen

Full paper

Highly-stable polymer-crosslinked 2D MXene-based flexible biocompatible electronic skins for in vivo biomonitoring

Lianjia Zhao [a], Lili Wang [b,*], Yiqiang Zheng [a], Shufang Zhao [b], Wei Wei [c], Dawei Zhang [d], Xiyao Fu [a], Kai Jiang [e], Guozhen Shen [b,*], Wei Han [a,*]

[a] Key Laboratory of Physics and Technology for Advanced Batteries (Ministry of Education), College of Physics, International Center of Future Science, Jilin University, Changchun 130012, China
[b] State Key Laboratory for Superlattices and Microstructures, Institute of Semiconductors, Chinese Academy of Sciences, Beijing 100083, China
[c] Laboratory of Theoretical and Computational Chemistry, Institute of Theoretical Chemistry, Jilin University, Changchun 130012, China
[d] School of Pharmaceutical Sciences, Jilin University, Changchun 130021, China
[e] Institute & Hospital of Hepatobiliary Surgery, Key Laboratory of Digital Hepatobiliary Surgery of Chinese PLA, Chinese PLA Medical School, Chinese PLA General Hospital, Beijing 100853, China

ARTICLE INFO

Keywords:
Electronic skins
PVA/MXene
Molecular dynamics calculations
Ultra-stable
Biocompatibility
In vivo study

ABSTRACT

The ability of electronic skins to identify physiological and physical signals accurately is the key to human-computer interaction. However, it is still a great challenge to improve stability of electronic-skin when maintaining the high-level pressure-response for applications in harsh conditions. Here, a highly-stable electronic skin is designed by synergistically incorporating strong hydrogen-bonds in MXene and polyvinyl alcohol (PVA). Molecular dynamics calculations show that the introduction of PVA can reduce the diffusion coefficient of MXene in acidic and basic solutions, increasing the adsorption (free) energies and providing hybrid film with good chemical stability. Therefore, the film provides stable performance recordings that last for over half a year in harsh environments. The film also shows good biocompatibility and function in an in-vivo study conducted on mice. To enhance functionality of soft robots and personal protective equipment used in harsh environments, it is important that the film has persistent and stable performance, all-weather usability, and good in vivo compatibility.

1. Introduction

Skin plays a vital role in shaping our interactions with the world [1–4]. When encountering harsh environments, the human skin could be damaged to varying degrees from the corrosiveness due to strong acidic or alkaline environment to causing the skin to lose its temporary sensing ability [5,6]. Resistance to skin damage ensures the safety of outdoor workers during operation in unpredictable environments. This scientific challenge has motivated the desire to develop highly stable electronic materials that can overcome the limitations of human skin under harsh conditions (acid, alkaline solution, hot water, *etc*.) and maintain their structure and properties [2,3,7]. Owing to unique sheet structure of two-dimensional (2D) materials at a single atomic thickness, the material can withstand more than 10% deformation before fracture, which is an order of magnitude higher than that of a typical bulk semiconductor, and the fracture value is usually <1%. The natural high flexibility of 2D materials has generated considerable interest in the field of flexible electronics [8–10]. Free-standing films fabricated by vacuum-assisted filtration of 2D material dispersions consist of random stacks of delaminated flakes; they show poor stability and resistance to strain because of the dissolution and sliding between the stacked 2D material flakes during mechanical deformations or harsh conditions [11]. However, in the applications of various electronic devices (such as electronic sensors), it is inevitable to encounter some natural dynamic environment, such as industrial wastewater (strong acid/strong alkali conditions) and underwater work [12]. Unfortunately, until now, the development of piezo-response films that are able to remain chemically and structurally stable under unpredictable surroundings remains a great challenge.

One of the strategies to overcome these challenges/constraints is to integrate polymers into conductive active materials and establish a strong interaction with (dynamic covalent or non-covalent bonds) to

* Corresponding authors.
E-mail addresses: liliwang@semi.ac.cn, lili_wang@jlu.edu.cn (L. Wang), gzshen@semi.ac.cn (G. Shen), whan@jlu.edu.cn (W. Han).

https://doi.org/10.1016/j.nanoen.2021.105921
Received 30 December 2020; Received in revised form 19 February 2021; Accepted 20 February 2021
Available online 26 February 2021

adjust the physical and chemical properties of 2D materials [12,13]. The physical and chemical properties are then adjusted/modified to develop strong, chemically stable, thin, flexible composite electronic films suitable for soft robot applications [14–16]. In this work, we used PVA as a crosslinker to connect the 2D $Ti_3C_2T_x$ MXene sheets (PVA/MXene) into a layered network structure through strong hydrogen bonding. This film exhibited chemically stable hierarchical structure and high piezoelectric response (Fig. 1a). The interaction (the diffusion coefficients ($D\alpha$)), potential of mean force (PMF), and adsorption (free) energies between materials were optimized by molecular dynamics calculation and experimental verification. PVA intercalation between MXene sheets was used to adjust the electrical characteristics and mechanical deformation ability (effective elastic modulus and hysteresis) of the materials and improve the strain recognition efficiency (sensitivity: 164.75 kPa^{-1}) and realize strong intermolecular interactions (strong hydrogen bonds). The introduction of biocompatible PVA improved the safety (excellent biocompatibility) of the device. This work shows that the use of electronic technology to reproduce the characteristics of skin provides a new direction for future soft robot and medical repair.

2. Experimental section

2.1. Materials

Titanium aluminum carbide powder (Ti_3AlC_2) was purchased from Jilin 11 Technology Co., Ltd. Lithium fluoride (LiF, AR, 99%) and

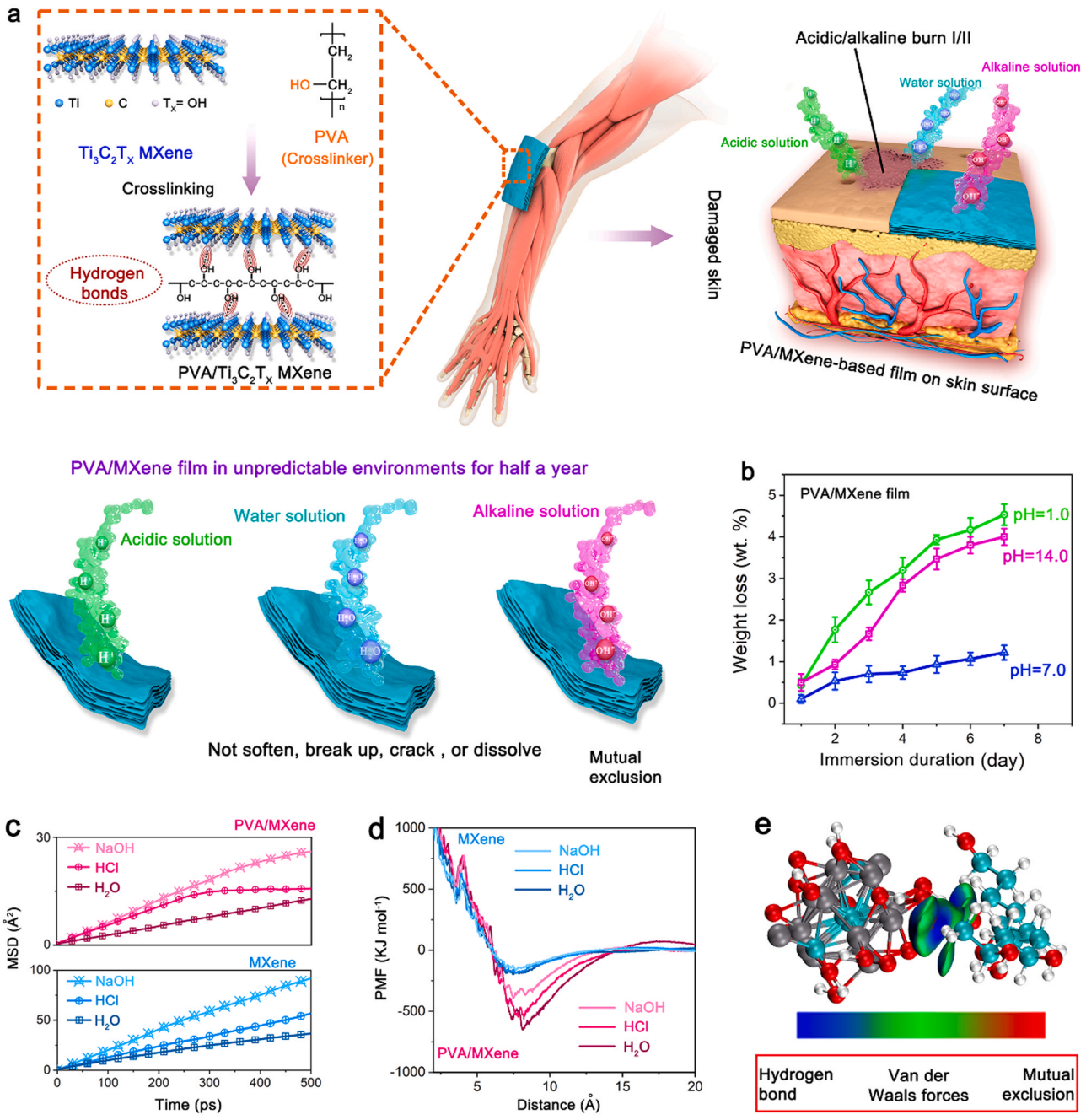

Fig. 1. Structures of the skin-like PVA/MXene hybrid thin film. (a) The schematic illustration of the skin-like PVA/MXene hybrid thin-film with crosslinked structures. (b) The weight losses of the PVA/MXene hybrid thin-films during the Immersion experiments at room temperature for 7 days ($n = 3$ measurements). (c) The MSD of the MXene and PVA/MXene hybrid thin-film in different solutions as a function of the simulation time. (d) The adsorption free energy of the MXene and PVA/MXene thin-film is shown in different solutions. (e) Natural bond analysis of PVA integrated with MXene in the HCl solution.

polyvinyl alcohol (PVA, Mw~ 145,000) were purchased from Aladdin Industrial Corporation. Hydrochloric acid (HCl, analytical reagent) and sulfuric acid (H_2SO_4, analytical reagent) were purchased from Beijing Chemical Works. All commercially available chemicals were used as received.

2.2. Synthesis of multilayer $Ti_3C_2T_x$ MXene powders

Multilayer $Ti_3C_2T_x$ MXene powder was prepared by selective etching the Al layer from Ti_3AlC_2 MAX. At room temperature (RT), 4.8 g of LiF was added to 60 mL of 9 M HCl, and then the mixture was stirred magnetically for 30 min to obtain a uniform solution. Subsequently, 3 g of Ti_3AlC_2 MAX powder was added to the previously prepared solution. The mixed solution was then magnetically stirred for 48 h at room temperature. The suspension thus obtained was diluted with deionized water and centrifuged at 3500 rpm for 5 min. To obtain multilayer $Ti_3C_2T_x$ MXene powders, the precipitate obtained by centrifugation was immersed in 60 mL of 2 M sulfuric acid for 30 min to remove excess LiF, and then the precipitate was washed with deionized water and centrifuged until the pH of the supernatant was above 6. The multilayer $Ti_3C_2T_x$ MXene powders were collected for the next experiment.

2.3. Synthesis of colloidal solutions of delaminated $Ti_3C_2T_x$ MXene flakes

A colloidal solution of delaminated $Ti_3C_2T_x$ MXene flakes was obtained by centrifuging an aqueous solution of multilayer $Ti_3C_2T_x$ MXene powders. The obtained powders were dissolved in 75 mL of deionized water and centrifuged at 3500 rpm for 10 min. The above procedures were repeated three times and the supernatant containing $Ti_3C_2T_x$ MXene flakes was collected each time for further film fabrication. The supernatant was a colloidal solution of delaminated $Ti_3C_2T_x$ MXene flakes, which is referred to as the $Ti_3C_2T_x$ MXene colloidal solution.

2.4. Fabrication of PVA/MXene hybrid solution

The hybrid solution was produced by adding a PVA aqueous solution to the $Ti_3C_2T_x$ MXene colloidal solution. First, 6 mg of PVA powder was added to 6 mL of deionized water and then heated for 4 h in an oven at 90 °C to completely dissolve the PVA powder. At the same time, 5 mL of the $Ti_3C_2T_x$ MXene colloidal solution was diluted with 40 mL of deionized water. Then, the obtained 6 mL of PVA aqueous solution (0.1 wt%) was slowly added to 45 mL of diluted $Ti_3C_2T_x$ MXene colloidal solution (~0.3 mg·mL^{-1}) and stirred for 1 h.

2.5. Fabrication of Free-Standing $Ti_3C_2T_x$ MXene and PVA/MXene films

Free-standing $Ti_3C_2T_x$ MXene and PVA/MXene films were fabricated via vacuum-assisted filtration of the corresponding solutions through a cellulose membrane (TJ JinTeng) with a diameter of 47 mm and a pore size of 0.22 nm. A solvent filter (TJ JinTeng), with a glass sand core, was used for vacuum filtration. The filtered membrane was dried for 30 min in a vacuum oven at 30 °C. The film formed was detached from the membrane.

2.6. Flexible pressure sensor fabrication

The pressure sensor was developed by sandwiching the PVA/MXene hybrid thin films on the surface of polyethylene terephthalate (PET) substrate with Au electrode. The PET substrate was washed with detergent, acetone, ethanol, and deionized water and dried in an oven before use. Two Ag wire electrodes were drawn out to facilitate experimental testing. To improve the stability and reliability of the measurement, a thin glass slide with an area of 150 mm^2 (15 mm × 10 mm) was placed on the PVA/MXene hybrid film-based flexible pressure sensors during the pressure-sensing tests. The flexible pressure sensor and the exposed electrode line (Ag wire) were encapsulated by using polydimethylsiloxane (PDMS) and then applied to different solutions for in vivo testing.

2.7. Sample characterization

X-ray diffraction (XRD) patterns were obtained with a powder diffractometer (DX-2700B) using Cu Kα radiation of wavelength k = 1.54056 Å at 40 kV, 30 mA and a step scan of 0.03° with 1 s per step. Scanning electron microscopy (SEM; Magellan 400) was used to obtain high-magnification images of the treated powders. Transmission electron microscopy (TEM) images were obtained using JEOL JSM–2010 F. For dynamic pressure measurements, a digital force gauge (Model SH-500, Capacity 500 N, SHANDU) with an Electric Horizontal Test Stand (SJX-500 V, SHANDU) were used to apply an external pressure, and the entire system was computer controlled. The current signals were tested using an A11719 Iviumstat electrochemical interface and CHI 760D (CH Instruments Inc., Shanghai, China) electrochemical workstation. Fourier transform infrared (FTIR) spectroscopy was performed with a Nicolet IS10 spectrometer to investigate the surface bonding of the materials. The atomic force microscope (Dimension Icon (Bruker, Germany)) was used to conduct the surface structure of materials. The composites were analyzed using X-ray photoelectron spectroscopy (XPS) (Thermo Escalab 250Xi).

2.8. Cell biocompatibility in vitro

Human umbilical vein endothelial cells (HUVECs) (Jennio Biotech Co. Ltd, GuangZhou, China) were sterilized under high temperature and pressure. HUVECs were suspended in the medium, and the HUVEC density was calculated as 4×10^5 cells mL^{-1} using a hemocytometer. The HUVECs were inoculated on a hybrid film with a density of 2×10^4 cells in the pores of the tissue culture plate and stored in a medium supplemented with 10% fetal bovine serum and 10% trypsin EDTA at 37 ºC in an incubator (SCO6WE, SHEL LAB) with 5% CO_2. The cells (HUVECs) were cultured in vitro for 24 (1 day), 72 (3 days) and 168 h (7 days), stained with 10 μL calcitonin-AM and 10 μL polyimide for 15–20 min, and then washed three times with phosphate-buffered saline (PBS). The cultured and stained HUVECs were placed on film and observed under fluorescence microscope (Leica DMI8, Germany). Data are represented as mean±S.D. (n = 10×10^5 cells/mL) examined over three independent experiments.

2.9. Preparation of the animal experiments and physiological signal recording in vivo

All animal experiments were conducted in accordance with the regulations of Jilin Provincial Science and Technology Department (approval number: 20200805–1). The experimental procedure was carried out according to the "Guide to the Care and Use of Experimental Animals". During the animal experiment, *BALB/c* mice (6–8 weeks old, 18–20 g) were anesthetized using Nembutal. The skin was incised to expose the epicardium of the heart. Next, a flexible pressure sensor was attached to the epicardium of the heart, and the three-point fixation method was used to anchor the pressure sensor to ensure that the device does not fall or move during heartbeat. However, the posture or position of the flexible sensor could be adjusted in the detection process because the contact flexible sensor moves during heartbeat. A similar process was used to anchor a sensor to the stomach wall to monitor gastric peristalsis. The flexible pressure sensor was attached to the tissues or organs to record the target signal. The TruEbox-01RC (TruEbox-01RC is a portable, continuous monitoring, cost-effective, user friendly and precise electrical tool (resistance/capacitance signal) for single/multi-channel device) was used to measure the signals at both ends of the sensor at a voltage of 1 V. Among them, the exposed electrode line in the body is coated by the passivation layer (PDMS). For quantification of the physiological signals, the sensitivity of the electronic signal was defined

as the ratio of the electronic signals (resistance value) during the mechanical motion to that during no mechanical motion.

3. Results and discussion

A highly stable electronic skin material was developed to overcome the corrosion limits of human skin in harsh environments (Fig. 1a). To create a hybrid thin film containing a strong interaction network, we first synthesized $Ti_3C_2T_x$ MXene (MXene) nanosheets containing a rich active group terminus (–OH) by selectively etching the Al elements of the Ti_3AlC_2 MAX precursor in HCl and LiF mixed solution (Fig. S1) [17, 18]. SEM and TEM images revealed that nanosheets with thicknesses of approximately few tens of nanometer, which were well-defined, nearly transparent, and relatively thin, are formed (Fig. S2). The X-ray scattering showed complete disappearance of the diffraction peak at 39°, and the (002) peak shifted to the left, indicating that Al was selectively removed from the Ti phase (Fig. S3) [19–21]. PVA, a polymer crosslinker [22], was added to the MXene nanosheets. The hydroxyl (-OH) in the PVA reacted with the -OH-terminated MXene surface and formed a strong hydrogen bond network and Ti−O−C bonds at the surface [23], which were identified by FTIR spectra. This indicates the successful incorporation of PVA crosslinker within the MXene nanosheet network (Fig. S4).

Immersion experiments in different solutions were performed on free-standing MXene films crosslinked with and without PVA to validate their chemical stability (Fig. 1b). MXene crosslinked with PVA to form a hybrid thin film that demonstrates excellent and long-term hydro-stability. This has been proved by performing in immersion tests for a duration of 7 days. Then, the films were dried in a vacuum drying oven at 30 °C overnight; the weight loss (1.2 ± 0.2 wt% in water, 4.0 ± 0.2 wt% in acid, and 4.5 ± 0.3 wt% in alkali solution,) was approximately 22–83-fold lower than the 100 wt% loss in pristine MXene films (Fig. 1b and Fig. S5). Moreover, the C=O groups from the FTIR spectra of the PVA crosslinked MXene films did not decrease during the drip-washing test, which is reflective of their high crosslinking degree and excellent hydro-stability (Fig. S6). Similar results were obtained in strong acidic and alkaline solutions, which indicates that good structural robustness and chemical stability of the PVA-crosslinked MXene films were far superior to those of pristine MXene films.

The interaction between the molecules is crucial for determining the stability of the sensing film for flexible electronics [24]. We performed molecular dynamics simulations to reveal the interactions between PVA and MXene (the surface charge and structure of the PVA and MXene are shown in Fig. S7) under different environments. The possible interaction mechanisms with the proposed molecular structures of the PVA/MXene films are illustrated in Fig. S8. The PVA chains can be entrapped in and bound to the MXene matrix to form 3D hydrogen-bonded PVA/MXene. Through these molecular dynamic simulations, the dynamic stability of the MXene matrix can be revealed in different solutions before and after PVA modification, that is, the diffusion coefficients (D_α, Fig. 1c) and PMF (Fig. 1d) of the MXene matrix under different solution conditions. In Fig. 1c, the mean square displacement (MSD) reveals that the D_α values of pristine MXene are high in water and acidic and alkaline solutions. The PVA/MXene hybrid thin films, however, interacted with each other, decreasing MXene diffusion speeds (Table S1) because of the difficulty to break the hydrogen bonds between the PVA hydroxyl groups and hydroxyl groups from the MXene matrix, even under strong acidic and alkaline solutions (Fig. 1e and Fig. S9). MXene is assumed to be fully hydrated; thus, in MSD simulations, MXene is more likely to move with hydration water molecules. Therefore, the MXene diffusion coefficient is faster than that of PVA/MXene. In addition to affecting the diffusion speeds, the combination of PVA and MXene also produces a strong interaction force. An analysis of the radial distribution function (RDF) between the two particles can provide the quantitative interaction force. Therefore, the RDFs between Ti_3C_2-OH molecules in water, acidic, and alkaline solution systems and those between Ti_3C_2-OH and PVA molecules in these three systems were calculated. The energies between the molecules mentioned above were determined by the PMF. The adsorption (free) energies, corresponding to minimum PMF, are shown in Fig. 1d and listed in Table S1. The energy of PVA/MXene under different conditions (−649.35 kJ mol^{-1} in water, −563.76 kJ mol^{-1} in acidic, and −390.78 kJ mol^{-1} in alkaline solution) are 2.3–3.2 times higher than that of pristine MXene (−198.34 kJ mol^{-1} in water, −188.75 kJ mol^{-1} in acidic, and −166.50 kJ mol^{-1} in alkaline solution). For systems containing water, acidic, and alkaline solutions, the strong interaction energy between PVA and MXene was difficult to weaken owing to the strong hydrogen bonds (Fig. 1e). In contrast, MXene nanomaterials without a PVA link are mainly connected by weak van der Waals forces (Fig. S9). However, the screening effect provided by the water molecules weakens the weak van der Waals force between the MXene molecules, resulting in the MXene thin film in various solutions to be less stable than that of the PVA/MXene thin film. Based on the unique hybrid crosslinked structures, the PVA/MXene hybrid thin film was soft and demonstrated structural robustness and strong mechanical performance.

The hierarchical structure plays a critical role in adjusting the compressive strain/deformation distribution within the support layer to avoid cracks triggered by the strain concentration while optimizing the crosslinked of the selective layer [25]. PVA/MXene can be easily regenerated through vacuum-assisted filtration (Fig. S10) to form a black-gray, paper-like, flexible thin-film (Fig. 2a) with a typical layered microstructure, as illustrated in the cross-sectional SEM image (Fig. 2b). Here, PVA is used as an intercalation agent to increase the interlayer spacing and form a large gap (Fig. 2b) and as interlocking agent to connect the MXene nanosheets (Fig. 2c) through hydrogen bonding, which was verified by XPS (Fig. 2d-f) and XRD (Fig. 2g). The obtained hybrid thin film is hydrophilic with a contact angle of approximately 55° (Fig. S11a) and is electrically conductive with a resistance value of approximately 6.25 kΩ (Fig. S11b). The interior structure consists of open pores with sizes ranging from 0 to 2 μm, which can be adjusted by the amount of PVA material used (Fig. S12). To further explore the bond structure and composite mechanism of the PVA/$Ti_3C_2T_x$ film, XPS spectra of the materials were obtained before and after the composite. A comparison of C 1s spectra (Fig. 2d) reveals that the C–Ti bond (281.7 eV) still exists after compounding, demonstrating that the layered structure of $Ti_3C_2T_x$ MXene is not destroyed during the compounding process. This result is consistent with the SEM images. After compounding, in addition to the existing C–C bond at 285 eV, a new C–C bond appeared at 284.4 eV, owing to the PVA. From the comparison of the O 1s spectra (Fig. 2e), the intensity of the O–Ti^{3+} bond (529.6 eV) increases after the composite, while the intensity of the O–Ti^{4+} bond (530.6 eV) decreases. The intensity of the Ti^{3+} bond (Ti^{3+} $2p_{3/2}$ at 456.5 eV and Ti^{3+} $2p_{1/2}$ at 462 eV) and Ti-O bond (458 eV) is enhanced, which is also caused by the reaction ($-OH + -OH = -O- + H_2O$) and formation of –C–O–Ti bonds (Fig. 2f) [22,26,27]. Thus, the XPS spectra coincide with the previous FTIR results and prove the formation of C–O–Ti bonds, and thus, the composite process did not damage the layered structure of.

$Ti_3C_2T_x$ MXene. The XRD results indicate that characteristic peaks of the pristine PVA appear in the PVA/MXene materials (Fig. 2g). Additionally, the (002) characteristic peaks of PVA/MXene shifted from 7.1° to 6.4° compared to the pristine MXene films, which suggested a uniform pillaring effect of PVA in the MXene matrix.

The mechanical properties of the PVA/MXene hybrid thin film were examined by adjusting the PVA content (Fig. S13). The 30% PVA/MXene hybrid thin film had an effective elastic modulus (E_{eff}, slope of the stress versus strain plot, 0.027 ± 0.002 MPa) lower than that of other PVA/MXene thin film and an open porous lamellar structure. Thus, 30% PVA/MXene was chosen for further testing. Compared with the pristine MXene thin film (2.87 ± 0.21 MPa), E_{eff} of the PVA/MXene thin film increased more than 100 times (Fig. 2h). Presumably, the elastic modulus was determined mainly by the structure of the film and

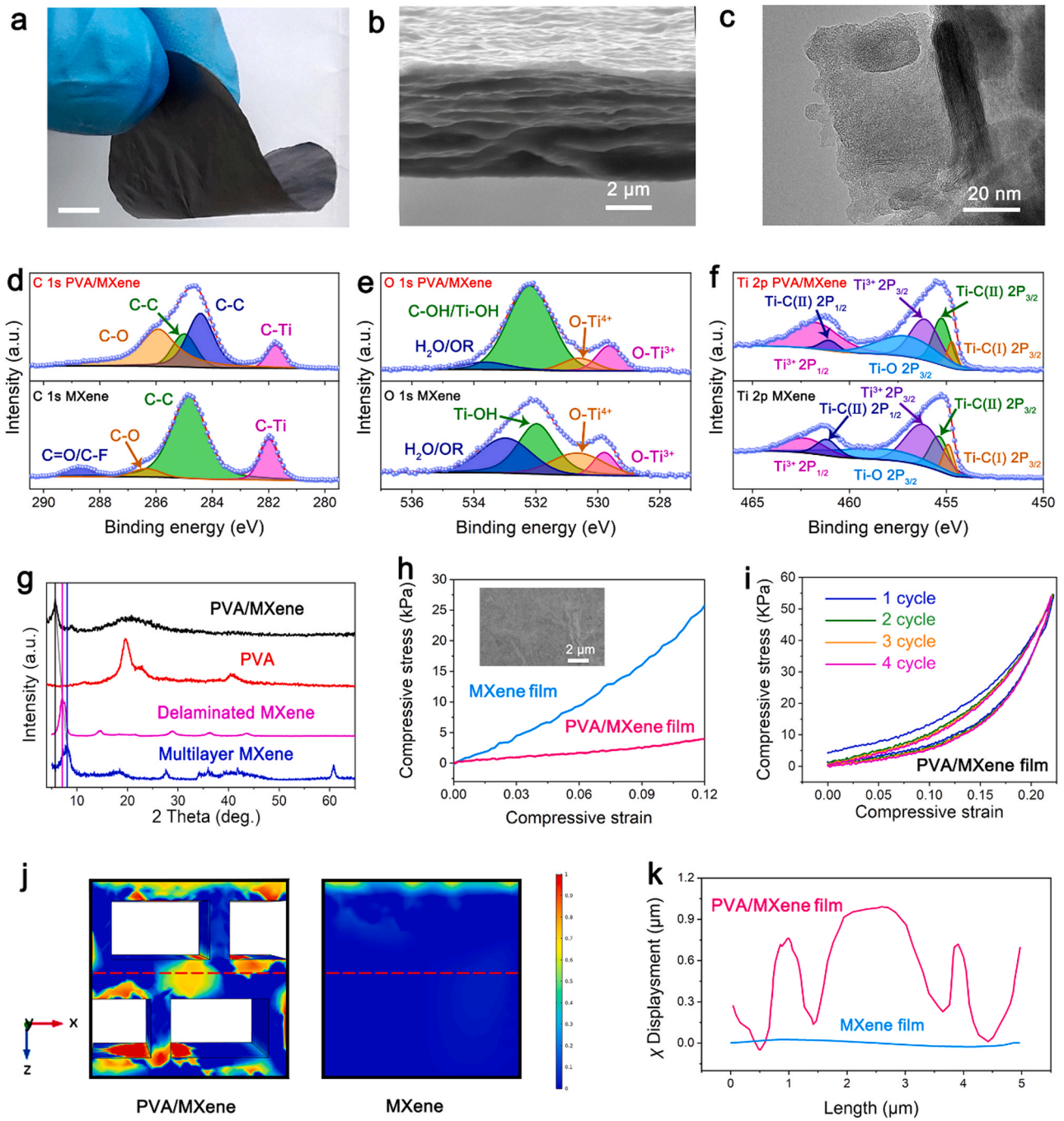

Fig. 2. Mechanical properties of the PVA/MXene hybrid thin film. (a) Optical, (b) cross-section SEM, and (c) TEM images of PVA/MXene hybrid thin-film (scale bar: 0.5 cm). The XPS spectrum analysis of PVA/MXene for (d) C 1s, (e) O 1s and (f) Ti 2p. (g) XRD pattern of pristine PVA, MXene and PVA/MXene. (h) Compressive stress–strain curves for pristine MXene and PVA/MXene thin-film. The inset shows the surface SEM image of the PVA/MXene hybrid thin-film. (i) Four consecutive compression tests on the PVA/MXene thin-film. (j) Cross-sectional view of FEM of the deformation distribution. (k) deformation distance (x) along the dashed red lines in (j).

hydrogen bonds. Conversely, when a force is applied, the resistance force of the hydrogen bonds can avoid cracks triggered by the strain concentration and result in a faster recovery [24,28]. Therefore, four consecutive compression tests were conducted under various strain levels to further prove the robust recoverability of the PVA/MXene hybrid thin film (Fig. 2i). The loading and unloading curves of the PVA/MXene thin film at compression stress (55 kPa) were superimposable and showed small hysteresis (7.3). However, the motion of dislocation in the open porous lamellated architecture is weaker than that in the structureless film. Such an open porous architecture could reasonably regulate the distribution of deformation (Fig. 2j) and force (Fig. S14) in this hybrid thin film. The finite element modeling (FEM) results indicated that the open porous structure exhibited more deformability inside the PVA/MXene thin-film compared to that in the pristine MXene film (Fig. 2k) [29]. Therefore, control of the molecular interactions makes the properties of the film programming reasonable, yielding high performance thin films with excellent low elastic moduli [15]. A good platform is offered for developing 2D-based hybrid films suitable in applications where mechanical strength and rapid recovery kinetics is required.

To validate the ability of PVA/MXene thin film to respond to external stimuli, a magnified view of the schematic of the e-skin, composed of PVA/MXene as the sensing layer, Au as the electrode, and PET as the flexible substrate, is shown in Fig. 3a. The typical response of the flexible pressure sensor, when gradually increasing the force on the sensors is shown in Fig. 3b. The step-by-step increase in the current signal confirms the ability of the flexible pressure sensor to monitor external force stimuli continuously [30]. The flexible pressure sensor also exhibits fast response and recovery features. The measured response and recovery times were approximately 29 and 31 ms, respectively (inset of Fig. 3b). In our system, the PVA/MXene thin-film-based flexible pressure sensor shows a wide range of pressure responses, up to 100 kPa (Fig. 3c), completely covering the working range of biological receptors. The pressure sensitivity (defined as the slope of the current change versus pressure ($S=\delta(\Delta I/I_0)/\delta p$), where $\Delta I=I-I_0$, I represents the pressure-induced change in current, I_0 represents the current without pressure loading and p represents the change in the applied pressure) is $164.75 \pm 0.4\ kPa^{-1}$ at lower pressures ($p < 35$ kPa) and $40.17 \pm 0.03\ kPa^{-1}$ at higher pressures ($35 < p < 100$ kPa). These values are one order of magnitude higher than those of the pristine MXene film (Fig. S15a) and better than that of previously published MXene sensors (Fig. S15b). The high sensitivity to low pressure is shown in Fig. S16, where a pressure as low as 0.11 Pa (corresponding to a grain of Styrofoam) can be accurately identified. To validate the pressure sensing property more intuitively, the pressure sensor can also drive a light-emitting diode (LED) to display different brightness [31–34]. When different pressures are applied to the sensor, the brightness of the LED bulb changes, as shown in Fig. S17. Furthermore, by using flexible pressure sensors, real-time, physical signal monitoring of swallowing, elbow flexion, and wrist, finger, muscle, and joint movement is successfully achieved, as illustrated in Fig. 3d–e and Fig. S18. The movement can be identified clearly by comparing the intensity and shape of the curves. As the main vital signs of human life, pulse signal detection offers medical information for a disease diagnosis. Fig. S19 (inset) shows a conformal skin sensor attached to the skin of the wrist for the real-time monitoring of the pulse cycle and waveform. Fig. 3f shows the pulse

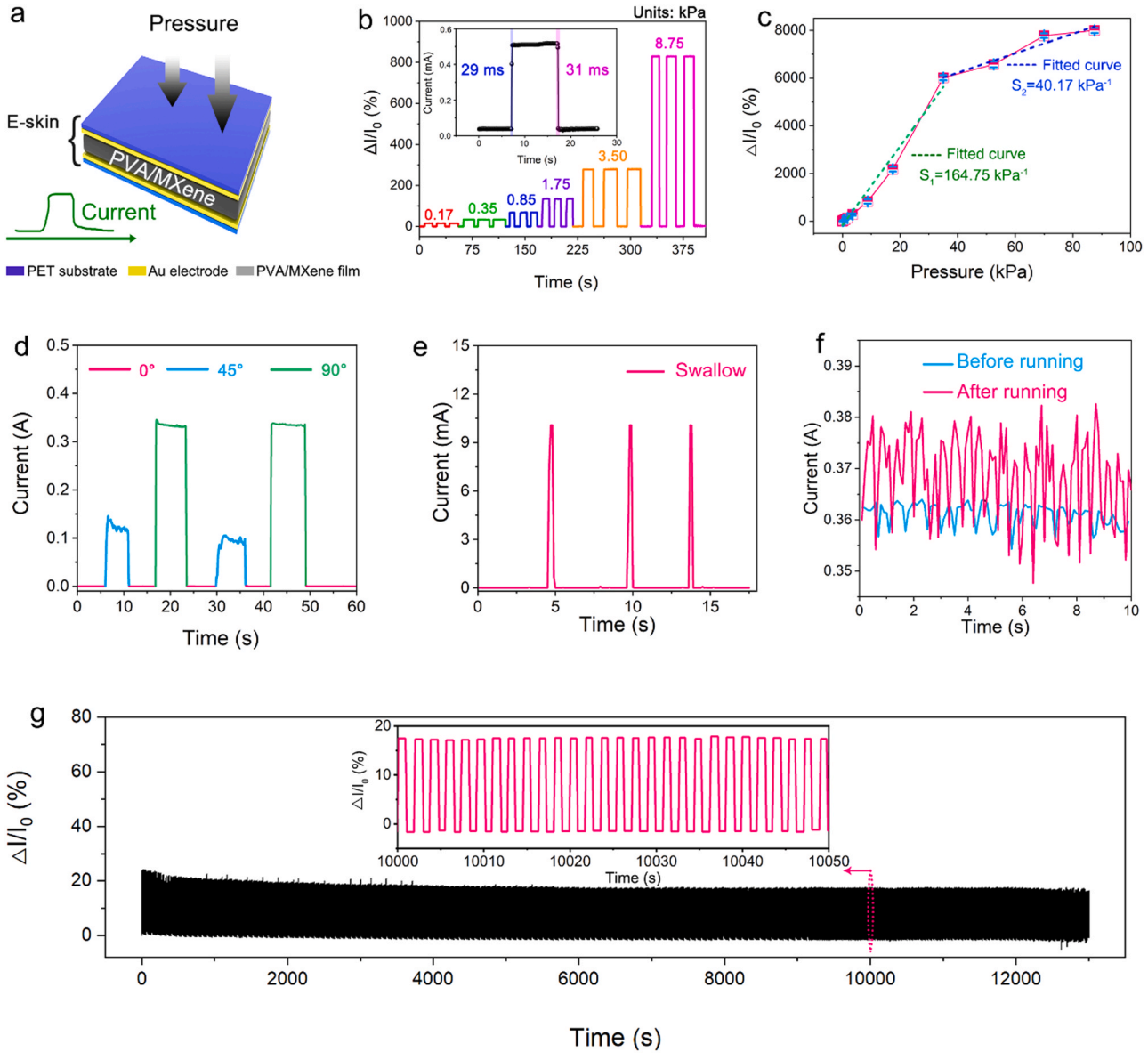

Fig. 3. Response characteristics of the pressure sensor. (a) Diagram of a pressure sensor. (b) A dynamic response curve and (c) sensitivity plots of the flexible sensors under various pressure levels ($n = 3$ measurements). The inset of (b) shows the response and recovery time. (d) The dynamic response curve to the bending angle (0–90°). (e) Detection of deglutition swallowing. (f) Pulse signal test before and after running. (g) Working stability tested over 7000 cycles at a pressure of 160 Pa.

signals of a male before and after running, and the characteristic peaks of the pulse waveform are clearly identified, indicating the high sensitivity of the sensor. Further, each pulse waveform contains two distinguishable characteristic peaks, P_1/P_2 and T, corresponding to percussion, tidal, and diastolic waves, respectively (Fig. S19) [15,35,36]. These flexible pressure sensors also show good durability during cyclic testing (7000 cycles) (Fig. 3g) and desirable response/recovery features during long-term continuous operation under loading-unloading conditions (inset of Fig. 3g). This sensing capability can meet the requirements for real-time biological monitoring in intensive medical rehabilitation training. In addition, a 5 × 5 sensor array was fabricated, which can successfully distinguish the location and shape of objects (Fig. S20).

To investigate stability under harsher conditions, a free-standing PVA/MXene thin film was immersed in water, acidic, and alkaline solutions for 8 weeks. The PVA/MXene free-standing film maintained a good film structure in water, acidic and alkaline solutions after 24 h of immersion (Fig. 4a and Fig. S21). The effective elastic modulus and hysteresis could be maintained at 98.6% ± 1.1% in water, 97.3% ± 1.3% in acidic, 96.9% ± 1.6% in alkaline solution and 95.0% ± 0.7% in water, 97.1% ± 0.8% in acidic, 96.8% ± 0.8% in alkaline solution after 24 h, respectively (Fig. 4b). After 8 weeks, the effective elastic modulus reached 0.048 ± 0.04% (Fig. 4c), 0.053 ± 0.05% (Fig. 4d) and 0.070 ± 0.06% (Fig. 4e) in water, acidic and alkaline solutions, respectively. This study shows an unparalleled mechanical stability of this hybrid thin film in a water/strong acidic/alkaline environment. The superiority of the effective elastic modulus in the PVA/MXene thin film compared to the pristine MXene thin film (Fig. 4f–h) is owing to the hydrogen bond crosslinks, which retain the mechanical cohesion longer in PVA/MXene. Because of the strong interaction between MXene and PVA (Fig. S9), the scope of its practical applications as a pressure sensor is high. It exhibited an average sensitivity of 61.7 (at 0.85 kPa) under

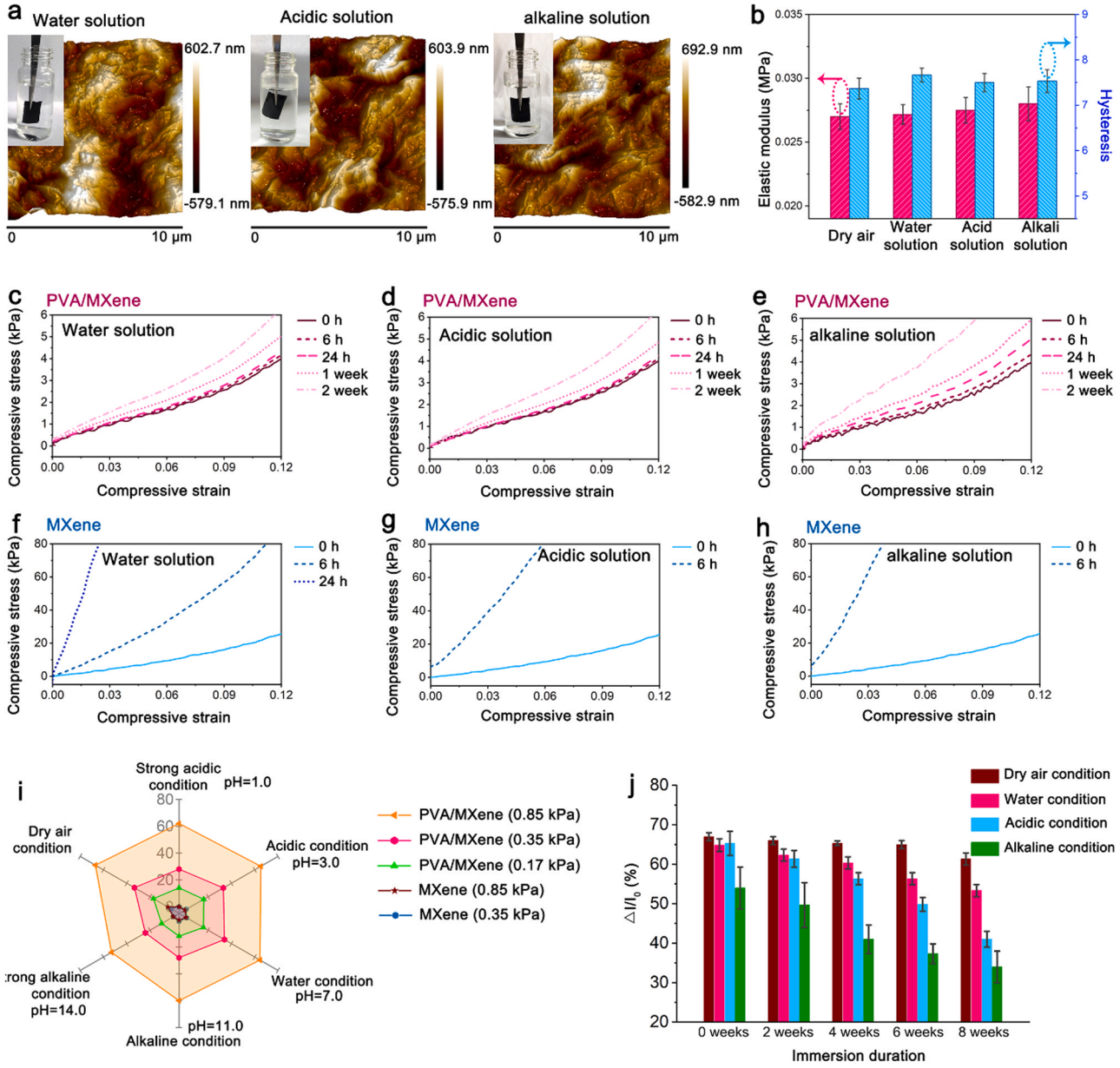

Fig. 4. Stability of the PVA/MXene thin-film. (a) atomic force microscopic (AFM) image of the PVA/MXene thin-film after immersion in different solution. (b) The effective elastic modulus and hysteresis study ($n = 3$ measurements). Compressive stress–strain characteristics for (c-e) PVA/MXene and (f-h) MXene under different solution for various immersion durations. (i) A comparison of the sensing performance to 0.17–0.85 kPa under different solution. (j) Long-term pressure response (0.85 kPa) study under different solution for various immersion durations (n = 3 measurements).

different environments (highest value after different washing solutions), which is higher than that of the pristine MXene flexible pressure sensor with a sensitivity of 2.8. Further, from the radar plot, it can be concluded that the hybrid thin film demonstrated good performance in all dimensions compared to that of the pristine MXene-based pressure sensor, which could cover only a few performance dimensions (Fig. 4i). To further confirm the stability of the hybrid thin film under harsher conditions, Fig. 4j shows the long-term stability of the hybrid thin film-based device under harsh conditions for 8 weeks. The pressure-sensitive performance of the flexible device deteriorated to varying degrees after immersion. After applying a constant pressure of 0.85 kPa for eight weeks, the device in dry air had the least degradation and the sensitivity was reduced by 8.5%. Meanwhile, in water, pH = 3, and pH = 11 solutions, the performance degraded by 17.7%, 32.6%, and 34.7% respectively. It can be seen that after eight weeks of immersion, the performance of all devices was maintained at more than 65%. Namely, when immersed in water, acid (pH = 3), and alkali (pH = 11) solutions, the final sensitivity was 53.3% ± 1.5%, 44.0% ± 3.6% and 34.6% ± 4.0%, respectively. These results indicated that the flexible pressure sensor based on PVA/MXene film has good stability in harsh environments. This hybrid thin film possessed excellent pressure sensitivity under a small external stimulus and good stability for over half a year in water and acidic/alkaline environments (Fig. S22), which is of great significance for expanding the application range of flexible electronic equipment in various environments.

In vitro and in vivo tests were conducted to prove that the pressure sensor has good biocompatibility and sensing functionality. To screen the biocompatibility and cytotoxicity of the constituent materials, we tested the cytocompatibility, viability, and growth of human umbilical vein endothelial cells (HUVECs) cultured on PVA/MXene. A tissue

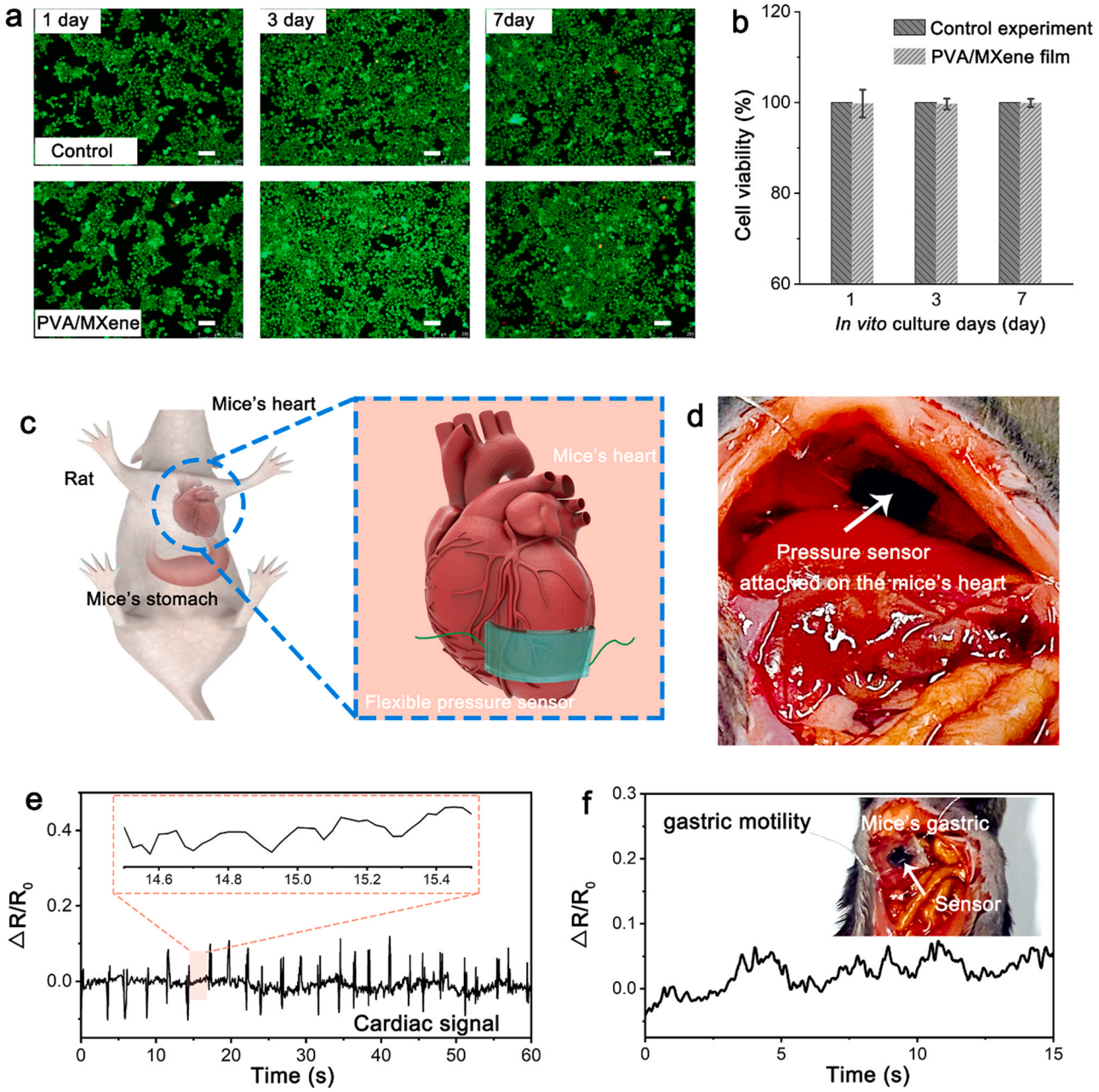

Fig. 5. Cell cytotoxicity tests and in vivo evaluation. (a) Fluorescent image of HUVECs cultured on PVA/MXene hybrid thin-film. (b) The cell viability over 1, 3, and 7 days (n = 3 measurements). Schematic (c) and photograph (d) of the pressure sensor attached to a mice' heart. (e) Measured electronic signal and (f) gastric dynamics study of the pressure sensor attached to a *balb/c* mice's heart and gastric wall.

culture of unused PVA/MXene was used as a control. The fluorescent images show the survival status of the cells in Fig. 5a. Cytotoxicity was not detected in a live/dead assay, and all surfaces had a large number of live cells (green) and a small number of dead cells (red), indicating that the majority of HUVECs are healthy (green in Fig. 5a). After 7 days (168 h), the survival rate of the human HUVECs was 99.8 ± 0.9%, and the number of HUVECs on the PVA/MXene film was not statistically different from that of the controls at the same time points (Fig. 5b). These data indicate that PVA/MXene has good biocompatibility in vitro, which is important for its use in biomedical applications.

For a biological sensing application, a flexible heart device is evaluated. The flexible and biocompatible pressure sensor was applied to the apical epicardium of the chest wall of a *BALB/c* mice (Fig. 5c and Video 1). In anesthetized *BALB/c* mice, the epicardial tip of the heart was exposed in the current experiment after the abdomen was dissected. The flexible pressure sensor was attached to the epicardial tip of the heart (Fig. 5d). Sutures were used to anchor the sensor at three points and keep the object in contact. This process avoids rigid attachment to minimize any restraint or change in heart movement. Similar suture techniques have been successfully applied to suture 3D patches on *BALB/c* mice left ventricular model, confirming that conformal contacts are maintained throughout the heart movement cycle from contraction to relaxation. The pressure sensor was linked to a home-made controller system (Fig. S23), which could transmit feedback electronic signals recorded from cardiac motion (see Methods). The changes in the electrical signals of the *BALB/c* mice heart owing to the heart-action-evoked potential were measured. Fig. 5e shows strong electrocardiograph (ECG) signals with high sensitivity and standard deviation. The gastric is another internal organ that is of interest in mechanical energy harvesting. Gastric peristalsis is the basis of gastric motility, which can be reflected by an electrogastrogram. After 30 min of feeding, the device was placed on the serous membrane of the outermost gastric wall, and the experimental results were as expected (Fig. 5f and Video 2). Therefore, these results indicate that the PVA-MXene-based flexible pressure sensor can easily utilize energy from different parts of the body, and the details of the operation depend on the species and organs [37–39].

Supplementary material related to this article can be found online at doi:10.1016/j.nanoen.2021.105921.

4. Conclusion

In this work, we demonstrate the fabrication of a biocompatible, highly stable, hybrid thin film comprising a PVA crosslinker and a highly conductive MXene nanosheet. We used a combination of a series of complementary experiments and molecular dynamics simulations to show that MXene films crosslinked with PVA by strong hydrogen bonds demonstrated the best structural stability (stable performance recording that lasts over half a year in acidic and basic aqueous solutions), mechanical properties (excellent elastic modules and minimal hysteresis), and pressure-sensing performances (ultra-high sensitivity and fast response time). In addition, we demonstrated the ability of this device to record in vivo cardiac signals in real-time and to monitor gastric peristalsis continuously in proof-of-concept mouse studies. The design of highly stable materials and devices has broad application prospects in the fields of artificial electronic skin, electronic medicine, and intelligent robots.

CRediT authorship contribution statement

Lianjia Zhao: Investigation, Methodology, Writing - review & editing. **Lili Wang:** Conceptualization, Investigation, Supervision, Funding acquisition, Project administration, Writing - review & editing. **Yiqiang Zheng:** Investigation, Writing - review & editing. **Shufang Zhao:** Software, Writing - review & editing. **Wei Wei:** Investigation, Writing - review & editing. **Dawei Zhang:** Investigation, Writing - review & editing. **Xiyao Fu:** Writing - review & editing. **Kai Jiang:** Supervision, Writing - review & editing. **Guozhen Shen:** Conceptualization, Supervision, Funding acquisition, Project administration, Writing - review & editing. **Wei Han:** Supervision, Funding acquisition, Project administration, Writing - review & editing.

Declaration of Competing Interest

The authors declare no competing interests.

Acknowledgment

We thank Prof. Y. Gogotsi and Prof. Z. Lou for valuable discussion. And thanks NICESCI Open Access Graphy for help with schematic design. We thank the authors sincerely acknowledge financial support from the National Natural Science Foundation of China (NSFC Grant No. 61874111, 61625404, 21571080, 61888102, 21903034), the Science and Technology Development Plan of Jilin Province (20190103135JH), Young Elite Scientists Sponsorship Program by CAST (2018QNRC001) and Foshan Innovative and Entrepreneurial Research Team Program (No. 2018IT100031).

Appendix A. Supporting information

Supplementary data associated with this article can be found in the online version at doi:10.1016/j.nanoen.2021.105921.

References

[1] X. Wang, L. Dong, H. Zhang, R. Yu, C. Pan, Z.L. Wang, Recent progress in electronic skin, Adv. Sci. 2 (2015), 1500169.
[2] S. Li, Y. Zhang, Y. Wang, K. Xia, Z. Yin, H. Wang, M. Zhang, X. Liang, H. Lu, M. Zhu, H. Wang, X. Shen, Y. Zhang, Physical sensors for skin-inspired electronics, InfoMat 2 (2019) 184–211.
[3] J.C. Yang, J. Mun, S.Y. Kwon, S. Park, Z. Bao, S. Park, Electronic skin: recent progress and future prospects for skin-attachable devices for health monitoring, robotics, and prosthetics, Adv. Mater. 31 (2019), 1904765.
[4] X. Peng, K. Dong, C. Ye, Y. Jiang, S. Zhai, R. Cheng, D. Liu, X. Gao, J. Wang, Z. L. Wang, A breathable, biodegradable, antibacterial, and self-powered electronic skin based on all-nanofiber triboelectric nanogenerators, Sci. Adv. 6 (2020), eaba9624.
[5] Y. Jie, J. Ma, Y. Chen, X. Cao, N. Wang, Z.L. Wang, Efficient delivery of power generated by a rotating triboelectric nanogenerator by conjunction of wired and wireless transmissions using Maxwell's displacement currents, Adv. Energy Mater. 8 (2018), 1802084.
[6] X. Cao, Y. Jie, N. Wang, Z.L. Wang, Triboelectric nanogenerators driven self-powered electrochemical processes for energy and environmental science, Adv. Energy Mater. 6 (2016), 1600665.
[7] A. Chortos, J. Liu, Z. Bao, Pursuing prosthetic electronic skin, Nat. Mater. 15 (2016) 937–950.
[8] S.J. Kim, K. Choi, B. Lee, Y. Kim, B.H. Hong, Materials for flexible, stretchable electronics: graphene and 2D materials, Annu. Rev. Mater. Res. 45 (2015) 63–84.
[9] H. Jiang, L. Zheng, Z. Liu, X. Wang, Two-dimensional materials: from mechanical properties to flexible mechanical sensors, InfoMat 2 (2019) 1077–1094.
[10] Y. Pang, Z. Yang, Y. Yang, T.L. Ren, Wearable electronics based on 2D materials for human physiological information detection, Small 16 (2020), 1901124.
[11] Z. Ling, C.E. Ren, M.Q. Zhao, J. Yang, J.M. Giammarco, J. Qiu, M.W. Barsoum, Y. Gogotsi, Flexible and conductive MXene films and nanocomposites with high capacitance, Proc. Natl. Acad. Sci. U.S.A 111 (2014) 16676–16681.
[12] F. Zhang, X. Lan, H. Peng, X. Hu, Q. Zhao, A "Trojan horse" camouflage strategy for high-performance cellulose paper and separators, Adv. Funct. Mater. 30 (2020), 2002169.
[13] L. Zhao, K. Wang, W. Wei, L. Wang, W. Han, High-performance flexible sensing devices based on polyaniline/MXene nanocomposites, InfoMat 1 (2019) 407–416.
[14] L. Zhao, Y. Zheng, K. Wang, C. Lv, W. Wei, L. Wang, W. Han, Highly stable cross-linked cationic polyacrylamide/Ti3C2TxMXene nanocomposites for flexible ammonia-recognition devices, Adv. Mater. Technol. 5 (2020), 2000248.
[15] K. Wang, Z. Lou, L. Wang, L. Zhao, S. Zhao, D. Wang, W. Han, K. Jiang, G. Shen, Bioinspired interlocked structure-induced high deformability for two-dimensional titanium carbide (mxene)/natural microcapsule-based flexible pressure sensors, ACS Nano 13 (2019) 9139–9147.
[16] D. Wang, L. Wang, Z. Lou, Y. Zheng, K. Wang, L. Zhao, W. Han, K. Jiang, G. Shen, Biomimetic, biocompatible and robust silk Fibroin-MXene film with stable 3D cross-link structure for flexible pressure sensors, Nano Energy 78 (2020), 105252.
[17] J. Nan, X. Guo, J. Xiao, X. Li, W. Chen, W. Wu, H. Liu, Y. Wang, M. Wu, G. Wang, Nanoengineering of 2D MXene-based materials for energy storage applications, Small (2019), 1902085.

[18] Q. Li, Q. Wang, L. Li, L. Yang, Y. Wang, X. Wang, H.-T. Fang, Femtosecond laser-etched MXene microsupercapacitors with double-side configuration via arbitrary on- and through-substrate connections, Adv. Energy Mater. 10 (2020), 2000470.
[19] M. Naguib, M. Kurtoglu, V. Presser, J. Lu, J. Niu, M. Heon, L. Hultman, Y. Gogotsi, M.W. Barsoum, Two-dimensional nanocrystals produced by exfoliation of Ti3AlC2, Adv. Mater. 23 (2011) 4248–4253.
[20] M. Naguib, V.N. Mochalin, M.W. Barsoum, Y. Gogotsi, 25th anniversary article: mxenes: a new family of two-dimensional materials, Adv. Mater. 26 (2014) 992–1005.
[21] X. Fu, L. Wang, L. Zhao, Z. Yuan, Y. Zhang, D. Wang, D. Wang, J. Li, D. Li, V. Shulga, G. Shen, W. Han, Controlled assembly of MXene nanosheets as an electrode and active layer for high-performance electronic skin, Adv. Funct. Mater. (2021), 2010533.
[22] S.A. Mirkhani, A. Shayesteh Zeraati, E. Aliabadian, M. Naguib, U. Sundararaj, High dielectric constant and low dielectric loss via poly(vinyl alcohol)/Ti3C2TxMXene nanocomposites, ACS Appl. Mater. Interfaces 11 (2019) 18599–18608.
[23] R. Liu, W. Li, High-thermal-stability and high-thermal-conductivity Ti3C2TxMXene/poly(vinyl alcohol) (PVA) composites, ACS Omega 3 (2018) 2609–2617.
[24] Y. Jie, Q. Jiang, Y. Zhang, N. Wang, X. Cao, A structural bionic design: from electric organs to systematic triboelectric generators, Nano Energy 27 (2016) 554–560.
[25] Z. Liu, X. Wang, D. Qi, C. Xu, J. Yu, Y. Liu, Y. Jiang, B. Liedberg, X. Chen, High-adhesion stretchable electrodes based on nanopile interlocking, Adv. Mater. 29 (2017), 1603382.
[26] S. Liu, L. Wang, X. Wang, L. Liu, A. Zhou, X. Cao, Preparation, mechanical and thermal characteristics of d-Ti3C2/PVA film, Mater. Today Commun. 22 (2020), 100799.
[27] C. Lu, L. Yang, B. Yan, L. Sun, P. Zhang, W. Zhang, Z. Sun, Nitrogen-doped Ti3C2MXene: mechanism investigation and electrochemical analysis, Adv. Funct. Mater. 30 (2020), 2000852.
[28] Y. Pan, L. Fu, Q. Zhou, Z. Wen, C.T. Lin, J. Yu, W. Wang, H. Zhao, Flammability, thermal stability and mechanical properties of polyvinyl alcohol nanocomposites reinforced with delaminated Ti3C2Tx(MXene, Polym. Compos. 41 (2019) 210–218.
[29] Z. Liu, X. Wang, D. Qi, C. Xu, J. Yu, Y. Liu, Y. Jiang, B. Liedberg, X. Chen, High-adhesion stretchable electrodes based on nanopile interlocking, Adv. Mater. 29 (2017), 1603382.
[30] Y. Ma, N. Liu, L. Li, X. Hu, Z. Zou, J. Wang, S. Luo, Y. Gao, A highly flexible and sensitive piezoresistive sensor based on MXene with greatly changed interlayer distances, Nat. Commun. 8 (2017) 1207.
[31] L. Wang, Z. Lou, K. Wang, S.F. Zhao, P.C. Yu, W. Wei, D. Wang, W. Han, K. Jiang, G.Z. Shen, Halide homogenization for high-performance blue perovskite electroluminescence, Research 2020 (2020) 1–10.
[32] Z. Ma, D. Kong, L.J. Pan, Z.N. Bao, Skin-inspired electronics: emerging semiconductor devices and systems, J. Semicond. 41 (2020), 041601.
[33] D.Y. Wang, L.L. Wang, G.Z. Shen, Nanofiber/nanowires-based flexible and stretchable sensors, J. Semicond. 41 (2020), 041605.
[34] Z. Wang, X.Y. Shan, X.G. Cui, P.F. Tian, Characteristics and techniques of GaN-based micro-LEDs for application in next-generation display, J. Semicond. 41 (2020), 041606.
[35] Z. Lou, S. Chen, L. Wang, R. Shi, L. Li, K. Jiang, D. Chen, G. Shen, Ultrasensitive and ultraflexible e-skins with dual functionalities for wearable electronics, Nano Energy 38 (2017) 28–35.
[36] L. Wang, J.A. Jackman, E.-L. Tan, J.H. Park, M.G. Potroz, E.T. Hwang, N.-J. Cho, High-performance, flexible electronic skin sensor incorporating natural microcapsule actuators, Nano Energy 36 (2017) 38–45.
[37] Y. Jie, H. Zhu, X. Cao, Y. Zhang, N. Wang, L. Zhang, Z.L. Wang, One-piece triboelectric nanosensor for self-triggered alarm system and latent fingerprint detection, ACS Nano 10 (2016) 10366–10372.
[38] M. Jo, K. Min, B. Roy, S. Kim, S. Lee, J.-Y. Park, S. Kim, Protein-based electronic skin akin to biological tissues, ACS Nano 12 (2018) 5637–5645.
[39] N. Gogurla, B. Roy, J.-Y. Park, S. Kim, Skin-contact actuated single-electrode protein triboelectric nanogenerator and strain sensor for biomechanical energy harvesting and motion sensing, Nano Energy 62 (2019) 674–681.

Lianjia Zhao received his B.S. degree in 2018 from Jilin University. He is a PhD candidate at the college of Physics, Jilin University, ChangChun, China. His research interests mainly focus on MXene/Polymer composite film-based flexible sensors and supercapacitors.

Lili Wang is a professor in the Institute of Semiconductors, Chinese Academy of Sciences, China. She earned her B. S. (2010) in Chemistry and Ph.D degree in Microelectronics and Solid State Electronics from Jilin University in 2014. Her current research interests focus on the flexible electronics based on biological materials, 2D materials and semiconductor, including pressure sensors, electronic-skin, biosensor, photodetectors and flexible energy storage and conversion devices.

Yiqiang Zheng received his B.S. degree in 2019 from Jilin University. He is a PhD candidate at the college of Physics, Jilin University, ChangChun, China. His research interests mainly focus on biomaterials-based flexible sensors.

Shufang Zhao is currently a Ph.D. candidate at Institute of Semiconductors, Chinese Academy of Sciences. Her current scientific interests focus on the design and manufacture of flexible electronic skin and artificial nerve synapses, and investigation of their fundamental properties.

Wei Wei is an Assistant Professor in the institute of theoretical chemistry at Jilin University, China. She earned his PhD degree in laboratory of theoretical and computational chemistry from Jilin University in 2014. Her current research interests focus on the theoretical calculation.

Dawei Zhang received his B.S. degree in Jilin University of China, Major in Biomedical Engineering. After that, I Worked 8 years as research assistant in Key Laboratory of Eco-Environmental Polymer Materials, Changchun Institute of Applied Chemistry, CAS. Then I joined Wish technology in 2017. And I will get my M.S. degree in 2020. His current research interests focus on the acute and Long-term toxicity of drugs and preclinical evaluation.

Xiyao Fu received her B.S. degree in 2017 from Jilin University. She is a PhD candidate at the college of Physics, Jilin University, ChangChun, China. Her research interests mainly focus on MXene composite film-based flexible electronics.

Kai Jiang received his MB/BS degree from Second Military Medical College, Shanghai, China, in 1991, and MD/PhD degrees from Chinese PLA Postgraduate Medical College, Beijing, China, in 1998. He further studied at the Queen Mary Hospital of University of Hong Kong in 2002, and Universitat de Barcelona, Spain, in 2008. He has been with the Faculty of Hepotopancreato-biliary Surgery, Chinese PLA General Hospital since 1991, where he is currently a Professor of surgery. His current research interests focus on surgical operation and applications of nanotechnology in clinical medicine.

Guozhen Shen received his BS degree (1999) in Chemistry from Anhui Normal University and PhD degree (2003) in Chemistry from the University of Science and technology of China. He joined the Institute of Semiconductors, Chinese Academy of Sciences, as a Professor in 2013. He has published more than 200 papers with a publication H-factor of 57. His current research focuses on flexible electronics and printable electronics, including transistors, photodetectors, sensors and flexible energy storage and conversion devices.

Wei Han received her B. S. degree (1993) in department of materials science from Jilin University and Ph. D degree (1997) in department of mechanical engineering from Tomsk Polytechnic University of Russia. He current research focused on energy storage materials and devices.